Performing spatial analysis on tropical cyclone rainband structures after creating a 3D Mosaic of WSR-88D reflectivity data using a map-reduce framework and a Geographic Information System (GIS)

BCS-1053864

Corene J. Matyas, Jingyin Tang, Stephanie E. Zick   Department of Geography, University of Florida

Introduction

Hurricane Isabel (2003) made landfall as a Category 2 storm at Drum Inlet, NC on Sept. 18 at 1700 UTC. We select Isabel for our analysis due to its large size and good predictions of track and extent of rainfall (NOAA 2003). As forecast models handled the system well, we hypothesize that our model simulation should be able to reproduce the intensity and spatial arrangement of rainbands. To test this hypothesis, we quantify the size, position, and spatial attributes of Isabel's rainfall regions near landfall for simulations of reflectivity from the Weather Research and Forecasting (WRF) model and Level II radar data from the Weather Surveillance Radar 1988 Doppler (WSR-88D) network that we mosaic to a 3D grid.

WSR-88D Reflectivity Processing

We employ a map-reduce framework (Lakshmanan and Humphrey 2014) to process Level II reflectivity data from radars within 600 km of the storm center (Fig. 1). After quality control and pre-processing, data are gridded at 250 m x 250 m x 250 m resolution every 5 minutes using data from a 10-minute moving window. Values for grid cells with data from multiple radars are calculated using a time-distance weighted function (Lakshmanan et al. 2006). Cells with missing values are filled using a distance-weighted interpolation performed in a Geographic Information System (GIS). We then draw contours every 5 dB*Z*, execute a smoothing algorithm, and convert the contours into polygons.

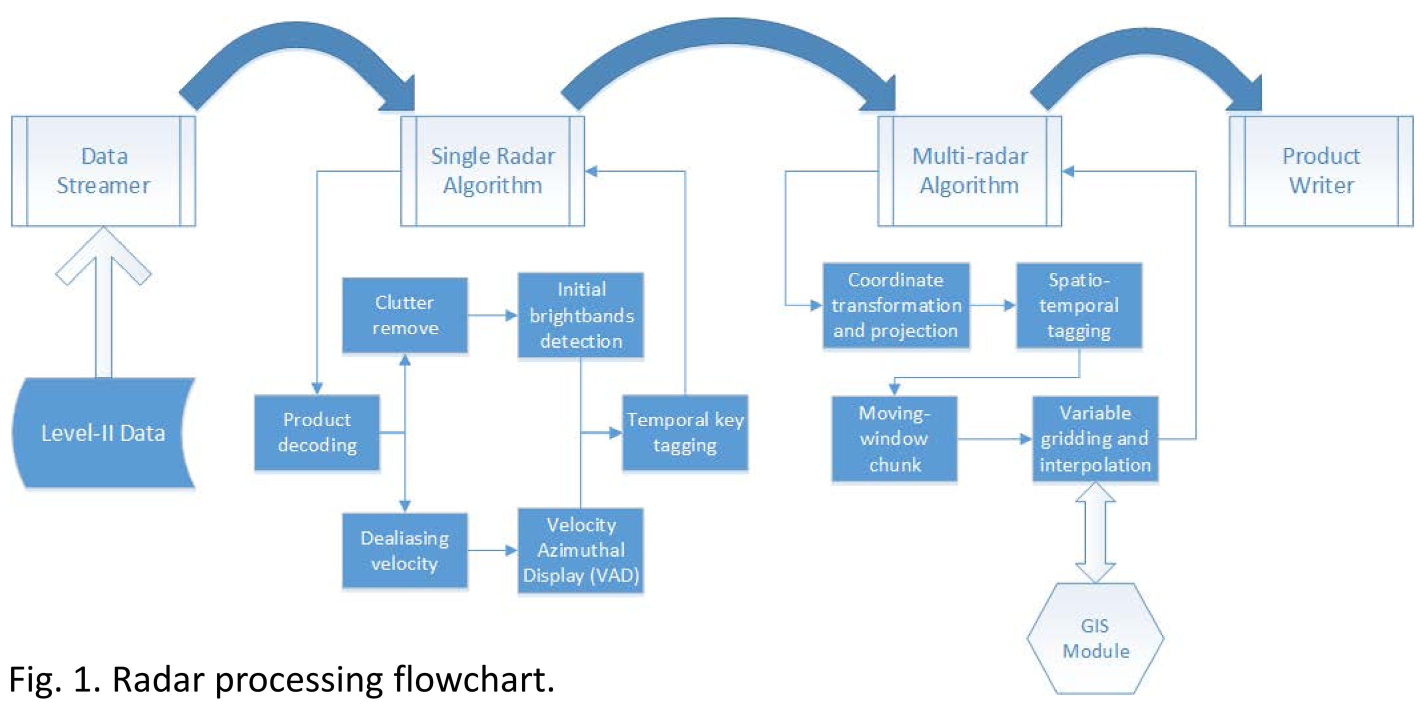

Fig. 1. Radar processing flowchart.

WRF Model Set Up

We utilize the Advanced Research Weather Research and Forecasting (WRF-ARW) model version 3.4.1 (Wang et al. 2012). The WRF model solves the fully compressible, non-hydrostatic Euler equations using a mass-based terrain-following vertical coordinate (Skamarock et al. 2008). The model domain is triply nested through two-way nesting with a coarse domain of 27 km horizontal resolution and two inner nests of 9 and 3 km resolution, respectively. The Global Forecast System final analyses are used for initial and boundary conditions. The coarse domain is initialized at 00 UTC Sept. 16, and inner nests are initialized 24 hours later. Modeling of tropical cyclones is highly sensitive to physical processes (e.g., Davis and Bosart 2002; Wang 2002). Also, simulated reflectivity depends on the model's microphysics scheme (Koch et al. 2005; Stoelinga 2005). We employ the following physics packages: WRF Single-Moment 6-class microphysics and Yonsei University (YSU) boundary layer scheme. The Tiedtke convective parameterization is utilized for 27 and 9 km simulations but turned off for the 3 km simulation. We examine simulated reflectivity every 30 minutes.

Shape Metric Calculations

We next quantify the spatial arrangement of polygons bounded by reflectivity values 20-45 dB*Z* every 5 dB*Z* (Fig. 2). The distance and bearing of polygon centroids are calculated relative to the storm center and used to measure fragmentation and dispersion (A) (Zick and Matyas 2014). Area is combined with perimeter to calculate compactness (B) (MacEachren 1985). The ratio of width to length permits calculation of elongation (C) (Maddox 1980) and orientation (Williams and Wentz 2008). Perimeter length is also used for convexity (D), which is the ratio between perimeters of the shape and its convex hull (Jamil et al. 1993). Determining the convex hull permits the calculation of solidity (E), which compares the shape's area to the area of its convex hull (Jiao et al. 2012). As TC rainbands tend to curve, we quantify the degree of closure around a circle for polygons that do not fully encircle the storm center (F) (Matyas and Tang 2015). We also calculate the percent of intersection between polygons produced by the WRF simulation and those from the radar observations. These measures help determine differences in rainfall regions and identify the best match of model to observations.

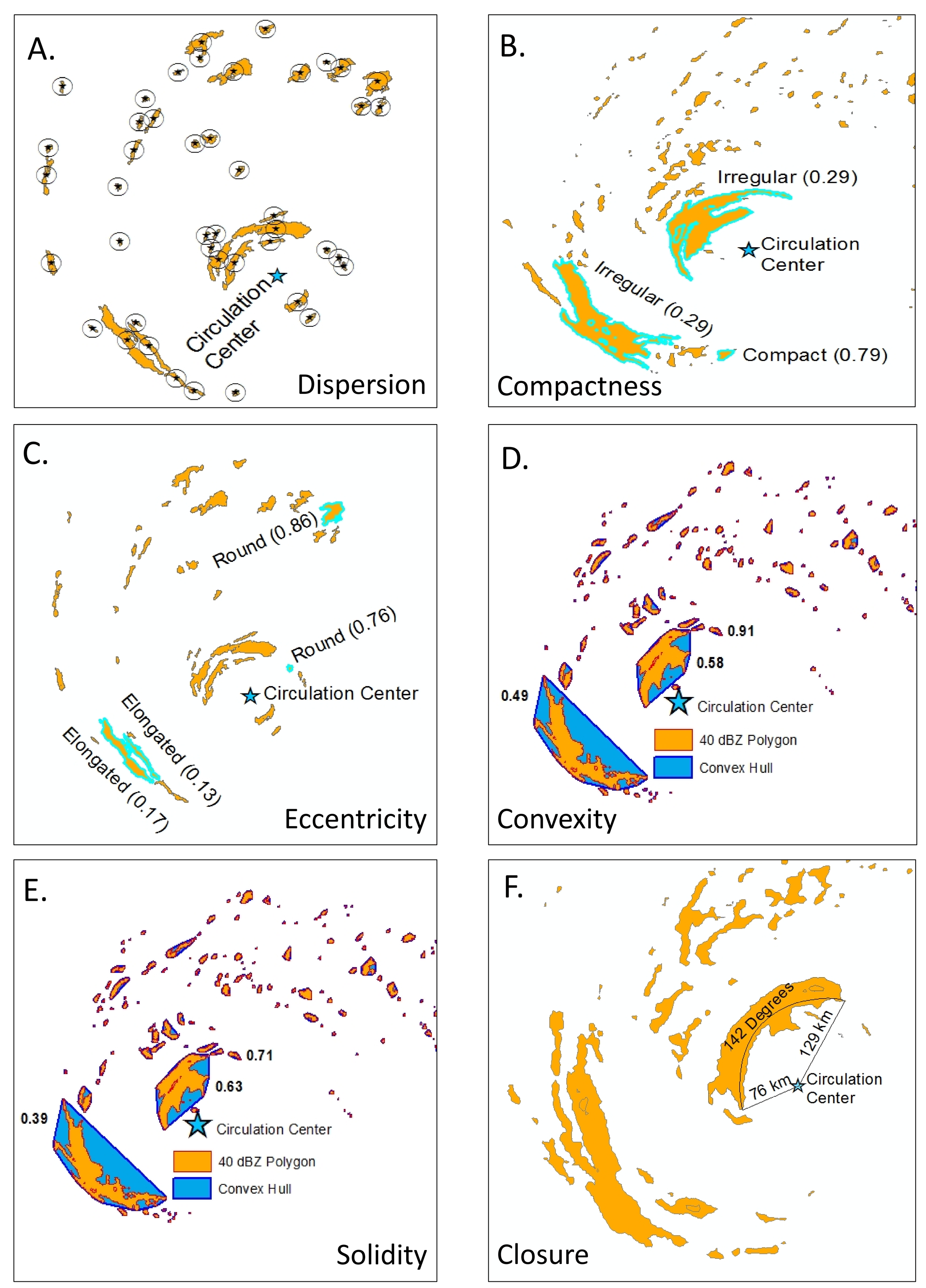

Fig. 2. Position and shape metrics identified in the paragraph above.

Results, Discussion, and Future Work

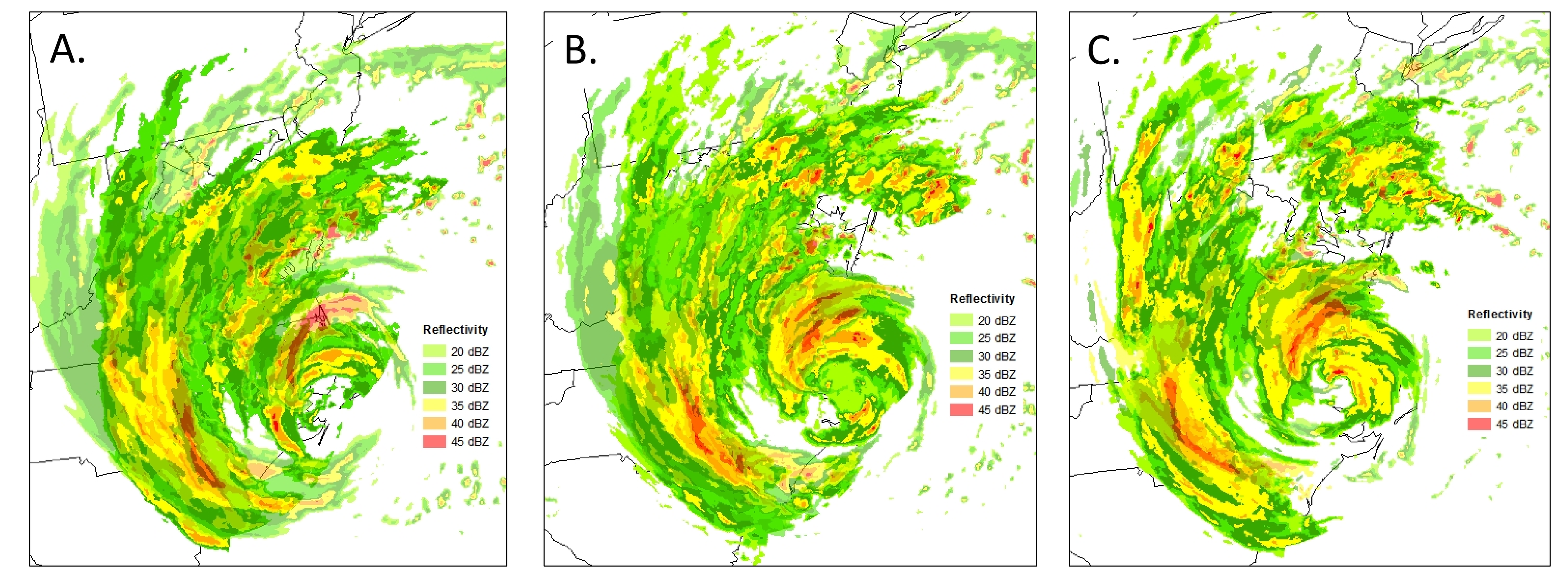

Fig. 3. 3.5 km reflectivity at A) 1700, B) 1830, C) 2000 UTC. WRF values are the transparent layer.

	n	B	C	D	E	F
Radar 1700	15	0.48	0.33	0.72	0.66	210°
WRF 1700	9	0.53	0.36	0.89	0.67	170°
Radar 1830	20	0.50	0.36	0.79	0.67	200°
WRF 1830	11	0.70	0.38	0.93	0.78	160°
Radar 2000	16	0.47	0.35	0.75	0.61	180°
WRF 2000	10	0.67	0.48	0.89	0.76	80°

Table 1. Median values for 40 dB*Z* (radar) and 45 dB*Z* polygons (WRF) with area >200 sq. km. Letters B-F correspond to Figure 2. Closure is for the storm core.

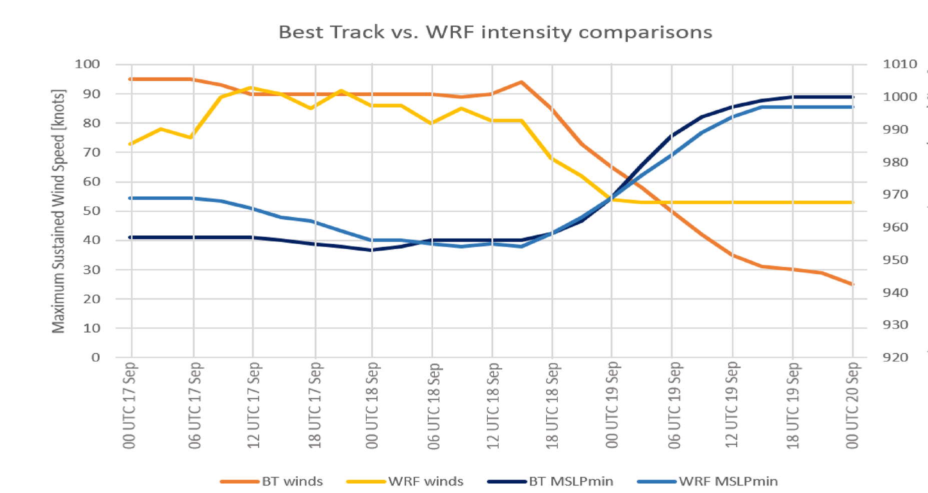

Fig. 4. Comparison of WRF minimum mean sea level pressure and maximum sustained wind speeds to the Best Track (BT). Time begins at inner nest initialization.

Although landfall occurred ~1 hour earlier and 120 km north in WRF, the high reflectivity polygons southwest of center have similar position and shape (Fig. 3a). At 1830 UTC, high reflectivity polygons surrounding the core are similar in shape and orientation despite the WRF centroid's offset of 60 km northwest (Fig. 3b). Yet, the model fails to produce the high reflectivity values over Maryland, which explains the increase in the number of radar-observed 40 dB*Z* polygons (Table 1). By 2000 UTC (Fig. 3c), WRF does not depict the broadening of the 35 dB*Z* region in the storm's core, a feature on radar also noted after Hurricane Charley's (2004) landfall (Matyas 2009). The model also moves the storm too quickly inland and exposes its core to environmental air more rapidly than was observed by radar (Table 1, column F), indicating an accelerated extratropical transition process (Gautam et al. 2008).

Due to model parameterization and resolution, we expected the WRF shapes to have less complex perimeters, yielding lower length values. Mann-Whitney *U* tests confirmed that compactness and convexity were significantly different between radar and WRF at each time. We did retain the null hypothesis of shape similarity for elongation, solidity, and orientation. Table 1 illustrates the similarity in elongation (C) and solidity (E), while the WRF shapes are more compact (B) with perimeters having similar lengths relative to their convex hull (D). Thus, we conclude that the calculation of shape metrics facilitates comparison of observed and modeled radar data.

Mann-Whitney *U* tests compared the shape metrics of the radar-observed 40 dB*Z* regions to the WRF 40 and 45 dB*Z* regions. Results show that the shapes of the 45 dB*Z* simulated regions were more similar to those of the observed 40 dB*Z* polygons, confirming that the WRF produced reflectivity values that were too high. Although the WRF simulation produced slower wind speeds, its minimum central pressure correlated highly with that of Isabel (Fig. 4), indicating a good representation of intensity. While we conclude that the WRF simulated reflectivity values accurately depicted shape and orientation, we hypothesize that the high reflectivity values may stem from the simplifying assumptions of a single-moment bulk microphysics scheme. Future work will investigate more complex microphysical parameterizations to better account for hydrometeor distributions.

References

- Davis, C., and L. F. Bosart, 2002: Numerical simulations of the genesis of Hurricane Diana (1984). Part II: Sensitivity of track and intensity prediction. *Mon. Weather Rev.*, **130**, 1100–1124
- Gautam, R., G. Cervone, R. P. Singh, and M. Kafatos, 2005: Characteristics of meteorological parameters associated with Hurricane Isabel. *Geophysical Research Letters*, **32,** Art. No. L04801.
- Jamil, N., Z. A. Bakar, and T. M. T. Sembok, 1993: Image retrieval of songket motifs using simple shape descriptors. *Geometric Modeling and Imaging--New Trends, 2006*, IEEE, 171-176.
- Jiao, L., Y. Liu, and H. Li, 2012: Characterizing land-use classes in remote sensing imagery by shape metrics. *ISPRS Journal of Photogrammetry and Remote Sensing*, **72,** 46-55.
- Koch, S. E., B. Ferrier, M. T. Stoelinga, E. Szoke, S. J. Weiss, and J. S. Kain, 2005: The use of simulated radar reflectivity fields in the diagnosis of mesoscale phenomena from high-resolution WRF model forecasts. 11th Conf. on Mesoscale Processes, Albuquerque, NM.
- Lakshmanan, V., and T. W. Humphrey, 2014: A MapReduce technique to mosaic continental-scale weather radar data in real-time. IEEE J. *Select Topics in Applied Earth Obs. & Remote Sensing*, 7, 721-732.
- Lakshmanan, V., T. Smith, K. Hondl, G. J. Stumpf, and A. Witt, 2006: A real-time, three-dimensional, rapidly updating, heterogeneous radar merger technique for reflectivity, velocity, and derived products. Wea. Forecasting, **21**, 802–823.
- MacEachren, A. M., 1985: Compactness of geographic shape: comparison and evaluation of measures. *Geografiska Annaler*, **67B,** 53-67.
- Maddox, R. A., 1980: Mesoscale convective complexes. *Bull. Amer. Meteor. Soc.*, **61,** 1374 - 1387.
- Matyas, C. J., 2009: A spatial analysis of radar reflectivity regions within Hurricane Charley (2004). *J. Appl. Meteor. Clim.*, **48,** 130-142.
- Matyas, C. J., and J. Tang, 2015: Measuring gaps in tropical cyclone rainbands using Level II radar reflectivity data. *69th Annual IHC meeting*, Jacksonville, FL.
- NOAA, Service Assessment: Hurricane Isabel, September 18-19, 2003. [http://www.weather.gov/os/assessments/pdfs/isabel.pdf.]
- Skamarock, W., J. Klemp, J. Dudhia, D. Gill, and D. Barker, 2008: *A description of the Advanced Research WRF version 3. NCAR Tech*. Note NCAR/TN-4751STR.
- Stoelinga, M. T., 2005: Simulated equivalent reflectivity factor as currently formulated in RIP: Description and possible improvements. *White Pap.*, **5**.
- Wang, W., D. Barker, J. Bray, C. Bruyere, M. Duda, J. Dudhia, D. Gill, and J. Michalakes, 2012: User's Guide for Advanced Research WRF (ARW) Modeling System Version 3.
- Wang, Y., 2002: An explicit simulation of tropical cyclones with a triply nested movable mesh primitive equation model: TCM3. Part II: Model refinements and sensitivity to cloud microphysics parameterization. *Mon. Weather Rev.*, **130**, 3022–3036,
- Williams, E. A., and E. A. Wentz, 2008: Pattern analysis based on type, orientation, size, and shape. *Geographical Analysis*, **40,** 97-122.
- Zick, S. E., and C. J. Matyas, 2014: Moisture budgets in U.S. landfalling tropical cyclones and implications for rainfall. *ICMCS-X meeting*, Boulder, CO.